Gyrotropic linear and nonlinear motions of a magnetic vortex in soft magnetic nanodots

Ki-Suk Lee and Sang-Koog Kim

Articles you may be interested in

Out-of-plane current controlled switching of the fourfold degenerate state of a magnetic vortex in soft magnetic nanodots
Appl. Phys. Lett. **96**, 072507 (2010); 10.1063/1.3310017

Understanding eigenfrequency shifts observed in vortex gyrotropic motions in a magnetic nanodot driven by spin-polarized out-of-plane dc current
Appl. Phys. Lett. **93**, 182508 (2008); 10.1063/1.3012380

Underlying mechanism of domain-wall motions in soft magnetic thin-film nanostripes beyond the velocity-breakdown regime
Appl. Phys. Lett. **93**, 052503 (2008); 10.1063/1.2968138

Formation and transformation of vortex structures in soft ferromagnetic ellipsoids
J. Appl. Phys. **103**, 07E739 (2008); 10.1063/1.2837499

Electric-current-driven vortex-core reversal in soft magnetic nanodots
Appl. Phys. Lett. **91**, 082506 (2007); 10.1063/1.2773748

Gyrotropic linear and nonlinear motions of a magnetic vortex in soft magnetic nanodots

Ki-Suk Lee and Sang-Koog Kim[a]

Research Center for Spin Dynamics and Spin-Wave Devices, and Nanospintronics Laboratory, Department of Materials Science and Engineering, College of Engineering, Seoul National University, Seoul 151-744, Republic of Korea

The authors investigated the gyrotropic linear and nonlinear motions of a magnetic vortex in soft magnetic cylindrical nanodots under in-plane oscillating magnetic fields of different frequencies and amplitudes, by employing both micromagnetic simulations and the numerical solutions of Thiele's equation of motion [Phys. Rev. Lett. **30**, 230 (1973)]. Not only noncircular elliptical vortex-core orbital trajectories in the linear regime but also complex trajectories including stadiumlike shape in the nonlinear regime were observed from the micromagnetic simulations and were in excellent agreement with the numerical solutions of the analytical equations of motion. It was verified that the numerical solutions of Thiele's equation are promisingly applicable in order to predict and describe well such complex vortex gyrotropic linear and nonlinear motions in both the initial transient and later steady states. These results enrich the fundamental understanding of the linear and nonlinear motions of vortices in confined magnetic elements in response to oscillating driving forces. © *2007 American Institute of Physics*. [DOI: 10.1063/1.2783272]

A magnetic vortex (MV), which consists of out-of-plane magnetizations (Ms) at its core region and in-plane curling Ms around the vortex core (VC), has been observed in continuous[1] or patterned[2,3] soft magnetic films. In addition to the unique static **M** configuration, it also has nontrivial dynamic properties such as the gyrotropic motion as verified by theory and experiments.[4–7] Hence the MV continues to grow in interest, especially because it is practically applicable to information storage owing to its thermal stability and tiny size (several tens of nanometer),[8,9] and is also applicable to resonators owing to the resonance of the MV motions under oscillating magnetic fields[10] or alternating electric currents.[11] More specifically, the VC in magnetic dots rotates around its center position with a certain eigenfrequency ν_0 that is determined by the dot geometry and material,[4–7] which is known as the gyrotropic motion with circular (no damping) or spiral (with damping) orbits in a finite-size magnetic element.[4] This motion, as studied theoretically, experimentally, and by simulations, is the simplest excitation mode among the MV excitations perturbed by pulsed magnetic fields,[5–7] oscillating magnetic fields,[10] and electric currents.[11]

Very recently, it has been found that the orientation of the VC (either up or down) can be switched dynamically not only by small-amplitude oscillating magnetic fields[12–15] but also by alternating currents.[16,17] Moreover, the physical origin and criteria for the dynamic switching are expected to be closely related to the VC gyrotropic motion.[14,17,18] Such low-power VC switching is considered to be an important step toward realizing high-performing magnetic memory devices using arrays of VCs.[9] Therefore, it is now crucially important to fundamentally understand the VC motions, particularly at resonance, including the linear and nonlinear motions driven by the alternating magnetic fields or currents. In this letter, we report results of micromagnetic simulations on VC gyro-tropic motions under oscillating in-plane magnetic fields, including not only elliptical trajectories and their shape change with the field frequency and amplitude but also complex VC trajectories in the initial transient state, and stadiumlike trajectories with small-amplitude circular orbits at both ends in the steady state. In order to interpret those simulation results we numerically solved Thiele's equations of motion[19] by assuming a "side-charge-free" model.[4]

In the present micromagnetic simulations and theoretical calculations, we used, as a model system, a cylindrical Permalloy [$Ni_{80}Fe_{20}(Py)$] nanodot of a diameter $2R=300$ nm and a thickness $L=10$ nm, as shown in Fig. 1(a). Using the OOMMF code[20] and a unit cell size of $2 \times 2 \times 10$ nm³ at the zero temperature, we investigated the **M** dynamics of an equilibrium vortex state with the downward core orientation in the nanodot under $\mathbf{H}(t)=A \sin(2\pi\nu t)\mathbf{y}$ with different frequency ν and amplitude A values, where the field is applied along the y axis.[14] For the Py material parameters, we used the saturation magnetization $M_s=8.6 \times 10^5$ A/m, the exchange stiffness $A_{ex}=1.3 \times 10^{-11}$ J/m, the damping constant $\alpha=0.01$, $\gamma=2.21 \times 10^5$ m/As, an anisotropic constant $K=0$. In Fig. 1(b), the VC orbital trajectories observed in the steady states are generally elliptical in shape, and their shape and size (amplitude) depend markedly on both ν and A. For example, for a relatively low A value (e.g., $A/A_s=0.2$), the ratio of the major to minor axis equals ν_0/ν or ν/ν_0, and the major axis is perpendicular (parallel) to the direction of the applied field for the case of $\nu < \nu_0$ ($\nu > \nu_0$)[21] [Fig. 1(c)]. Here, the eigenfrequecy and the static annihilation field are estimated to be $\nu_0=330$ MHz and $A_s=500$ Oe, respectively, in the given dot and geometry. The circular orbit[10,11] for $\nu=\nu_0$ is a specific case of these elliptical orbits. For the given $\nu/\nu_0=0.3$, however, the size of the orbital ellipse increases with increasing A (Ref. 14). For a sufficiently large A (e.g., $A/A_s=0.6$), the VC trajectory shape is stadiumlike with smaller-amplitude circular orbits at both ends of the major axis.

---
[a]Author to whom correspondence should be addressed. Electronic mail: sangkoog@snu.ac.kr
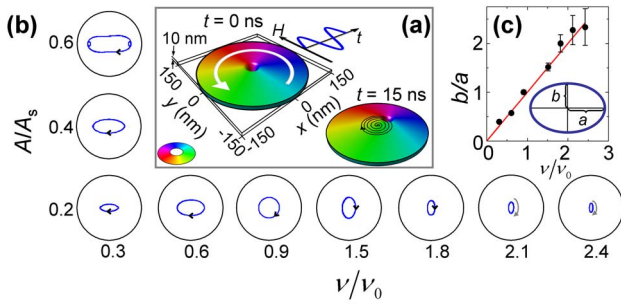
FIG. 1. (Color online) (a) Geometry and coordinates of the model Py nanodot along with the corresponding **M** configurations at the indicated times. The top- and bottom-perspective snapshot images display the initial equilibrium ($t=0$ ns) and the dynamic ($t=15$ ns) MV states with the downward core orientation and counterclockwise in-plane rotation. The color and height of the surface indicate the in-plane and out-of-plane **M** components, respectively. The spiral like black line on the right denotes the orbital trajectory of VC motion during the time period of $t=0-15$ ns with $A=10$ Oe and $\nu=\nu_0=330$ MHz. (b) Orbital trajectories of VC motions for the indicated A and ν values. (c) The aspect ratio (b/a) of the elliptical orbits vs ν/ν_0 for the case of $A/A_s=0.2$. The red line indicates the case of $b/a = \nu/\nu_0$,[21] where a and b are the lengths of the ellipse along the x (perpendicular to the **H** direction) and y (along the **H** direction) axes, respectively.
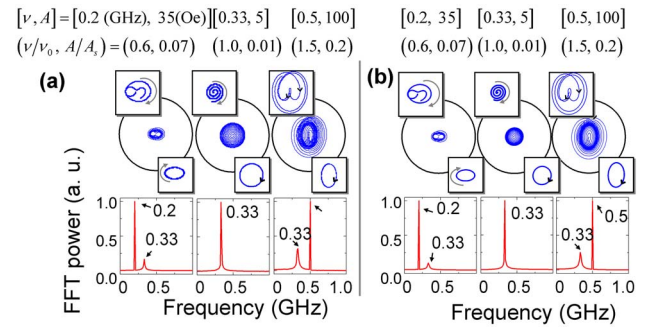

FIG. 2. (Color online) VC trajectories and their FFT powers under in-plane oscillating fields with various ν's and A's, as noted. For comparison, the micromagnetic simulation results and the numerical solutions of the linearized equation of motion $[-\mathbf{G}\times\dot{\mathbf{X}}-\hat{D}\dot{\mathbf{X}}+\kappa\mathbf{X}-\mu(\hat{z}\times\mathbf{H})=0]$ are shown in (a) and (b), respectively. The VC trajectories shown in the whole area of the dot were drawn during the time interval of $t=0-100$ ns, but in the upper left during $t=0-10$ ns, and in the lower right during $t=90-100$, $94-100$, and $96-100$ ns in order from the first to third column, respectively. The magnitudes of the FFT powers were normalized by the maximum value of each case.

Simulation results on the VC trajectories of vortex motion for both earlier transient and later steady-states, as well as their frequency spectra are shown in Fig. 2(a). For each case of the field parameters as noted, the VC starts to move from its initial center position with the corresponding complex orbit in the transient state (upper left side), and then reaches a steady state with the elliptical orbit of a characteristic shape, (lower right) depending on both ν and A. For the case of $\nu=\nu_0$, the transient motion is spiral-like, and the steady motion is of a single circular orbit. To elucidate such complex gyrotropic motions to different field parameters, we plotted their frequency spectra from the fast fourier transforms (FFTs) of the time evolution of the x component of the VC position, obtained from micromagnetic simulations, as shown in the bottom of Fig. 2(a). In the frequency spectra there exist only two main peaks: one is a sharp high peak at the corresponding external field frequency ($\nu=0.2$, 0.33, and 0.5 GHz) and the other is a small, relatively wide peak at $\nu_0=330$ MHz. For the special case of $\nu=\nu_0$, the driving-field-corresponding and eigenfrequency peaks are overlapped. Since the steady-state motions are driven by the externally applied oscillating fields, the sharp peak corresponds to this steady-state motion. The other peak at $\nu=\nu_0$ corresponds to the initial transient motion that results from the VC resonant excitation in the given dot. It is interesting that the transient complex VC motions observed from the micromagnetic simulations have only one frequency, i.e., ν_0. This indicates that the transient VC motion, which appears to be complex or chaotic, is not chaotic but predictable with an effective equation of motion for the vortex collective coordinates.

In order to analytically interpret the field-parameter dependent VC motions and their underlying physics, we first consider small-amplitude orbital motions corresponding to the gyrotropic linear regime. Assuming that **M** distributions in the dot are independent of the z coordinate along the dot thickness [i.e., two-dimensional model (see Ref. 6)], the vortex motion can be described by an effective Thiele's equation of motion for vortex collective coordinates,[19] which can be derived from the Landau-Lifshitz equation of motion, yield-

ing $-\mathbf{G}\times\dot{\mathbf{X}}-\hat{D}\dot{\mathbf{X}}+\partial W(\mathbf{X})/\partial\mathbf{X}=0$, where $\mathbf{X}=(X,Y)$ is the VC position, $W(\mathbf{X})$ is the potential energy of the VC shifted from its equilibrium position ($\mathbf{X}=0$), $\mathbf{G}$ is the gyrovector,[4] and $\hat{D}$ is the damping tensor.[10] For an appropriate description of the shift of the VC from $\mathbf{X}=0$, we used the side-charge-free model,[4] which shows good agreement between micromagnetic simulations[4] and experimental results[7] for the vortex translational mode for the cases of thin dots. For a cylindrical dot under nonzero external fields, the function $W(\mathbf{X})$ can be written as $W(\mathbf{X})=W(0)+\kappa\mathbf{X}^2/2+O(\mathbf{X}^4)-\mu[\hat{z}\times\mathbf{H}]\cdot\mathbf{X}$, where κ is the stiffness coefficient and a function of R and L, $\mu=\pi RLM_s\xi C$, $\xi=2/3$, and C is the vortex chirality.[4,10] The linearized equation of the VC motion, including the damping and Zeeman terms, is finally given as $-\mathbf{G}\times\dot{\mathbf{X}}-\hat{D}\dot{\mathbf{X}}+\kappa\mathbf{X} -\mu(\hat{z}\times\mathbf{H})=0$. By using the Runge-Kutta method to solve the initial value problem for such an ordinary differential equation, we obtained the numerical solutions as shown in Fig. 2(b). The simulation results and numerical solutions are in quite good agreement, both in the steady state and initial transient states.

Next, to understand the stadium shape of a VC orbital trajectory shown in Fig. 1(b), we plotted the VC trajectories of the gyrotropic motion in the different time intervals in response to the field with $A=300$ Oe and $\nu=100$ MHz in Fig. 3(a). These orbital trajectories in the transient state ($0-10$ ns) and the steady state ($80-100$ ns) are more complex than simple circular or elliptical orbits. As seen in Fig. 3(b), there exist four peaks rather than two peaks in the frequency spectrum. To identify each peak, we made inverse FFTs of the FFT powers in the individual frequency regions indicated by the different colors.[22] As the results of the inverse FFTs, the VC trajectories corresponding to the individual peaks and their superposition are plotted in the upper and lower rows in Fig. 3(c), respectively. The main, largest peak at $\nu=100$ MHz and its next two harmonics of 3ν and 5ν correspond to the steady-state motions as the nonlinear responses to the driving field of a frequency ν. In contrast, the relatively broad peak at 440 MHz between the 3ν and 5ν peaks corresponds to the initial transient motion caused by the vortex eigenmotion, which is shifted from $\nu_0=330$ (for the linear case) to 440 MHz due to the significant non-

(a)

$t = 0 \sim 100$ ns $0 \sim 10$ ns $80 \sim 100$ ns

(b)

Δf_1 Δf_2 Δf_0 Δf_3

(c) Δf_1 Δf_2 Δf_3 Δf_0

$\Delta f_1 + \Delta f_2$ $\Delta f_1 + \Delta f_2 + \Delta f_3$ $\Delta f_1 + \Delta f_2 + \Delta f_3 + \Delta f_0$
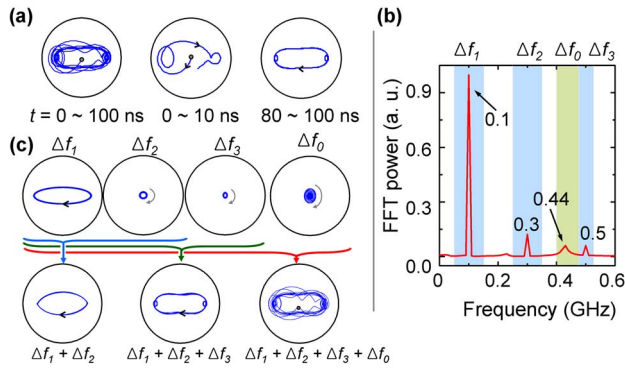
FIG. 3. (Color online) (a) Simulation results of the VC trajectories of the gyrotropic motion in different time periods as noted, and (b) the FFT power spectrum for the case of $\nu/\nu_0 = 0.3$ ($\nu = 100$ MHz) and $A/A_s = 0.6$ ($A = 300$ Oe). (c) Identification of the individual peaks (marked by colored regions) in the FFT power spectrum in (b). Each VC trajectory shown in the first row was obtained from the inverse FFTs of the frequency powers in each range of $\Delta f_1 = 50$–150 MHz, $\Delta f_2 = 250$–350 MHz, $\Delta f_3 = 475$–525 MHz, and $\Delta f_0 = 400$–475 MHz, as displayed by the color-coded regions in the frequency spectrum. The second row denotes the superposition of the filtered VC trajectories corresponding to the individual frequency regions.

linearity. In Thiele's equation of motion, this nonlinearity of large-amplitude VC gyrotropic motion is due to some higher-order energy terms in the function $W(\mathbf{X})$. To analytically interpret such nonlinear motions using Thiele's equation of motion, we added a fourth-order term ($\beta\mathbf{X}^4/4$) into the $W(\mathbf{X})$ yielding $-\mathbf{G}\times\dot{\mathbf{X}} - \hat{D}\dot{\mathbf{X}} + \kappa\mathbf{X} + \beta\mathbf{X}^3 - \mu(\hat{\mathbf{z}}\times\mathbf{H}) = 0$. The numerical solutions of this equation for different β's are shown in Fig. 4. The number of peaks, and their position and magnitude in the frequency spectrum dramatically change with β. For a specific value of $\beta/\kappa = 4.5\times10^{13}$ m^{-2}, not only the

$\beta/\kappa = 0$ (m^{-2}) 1.0×10^{13} 4.5×10^{13} 11.0×10^{13}
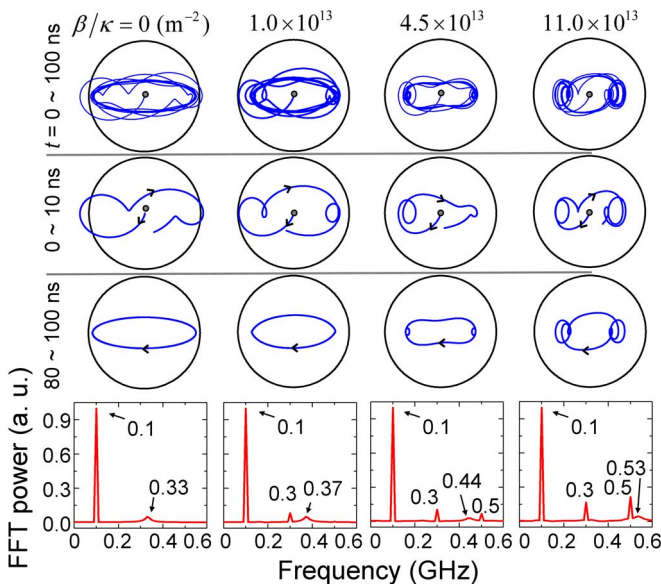

FIG. 4. (Color online) VC trajectories in different time periods as indicated, all of which were obtained from the numerical solutions of $-\mathbf{G}\times\dot{\mathbf{X}} - \hat{D}\dot{\mathbf{X}} + \kappa\mathbf{X} + \beta\mathbf{X}^3 - \mu(\hat{\mathbf{z}}\times\mathbf{H}) = 0$ for the different values of β/κ, as noted above each case (column), for the same oscillating field parameters as in Fig. 3, i.e., $\nu/\nu_0 = 0.3$ and $A/A_s = 0.6$. The bottom row shows the FFT spectra corresponding to the VC motion in the time interval of $t = 0$–100 ns. The FFT power spectra were normalized by the maximum value in each case.

trajectories but also the frequency spectra obtained from the numerical solution (the third column of Fig. 4) are in best agreement with those from the simulation [Fig. 3(a)]. With increasing β the number of harmonic peaks and their intensities, and the shift of the eigenfrequency of the VC motion increase (see Fig. 4). The extent of the nonlinearity of the VC motion can be represented by the magnitude of β. The shape of the stadiumlike orbit with the small-amplitude circular orbits at both ends is surely the result of the nonlinearity of VC motions, as evidenced by the higher-order term included in the $W(\mathbf{X})$. Such complex VC motion, including the initial transient and the steady-state motions, can be well interpreted or reproduced using Thiele's equation of motion by taking into account the higher-order potential energy terms.

In conclusion, the results presented in this letter not only offer a simple and easy way to investigate linear and nonlinear vortex-core gyrotropic motions but also open up an opportunity to manipulate vortex-core gyrotropic motions in given soft magnetic nanoelements by changing the field frequency and amplitude of in-plane oscillating driving forces such as a magnetic field.

[1] S.-K. Kim, K.-S. Lee, B.-W. Kang, K.-J. Lee, and J. B. Kortright, Appl. Phys. Lett. **86**, 052504 (2005).

[2] T. Shinjo, T. Okuno, R. Hassdorf, K. Shigeto, and T. Ono, Science **289**, 930 (2000); A. Wachowiak, J. Wiebe, M. Bode, O. Pietzsch, M. Morgenstern, and R. Wiesendanger, *ibid.* **298**, 577 (2002).

[3] R. P. Cowburn, D. K. Koltsov, A. O. Adeyeye, M. E. Welland, and D. M. Tricker, Phys. Rev. Lett. **83**, 1042 (1999).

[4] K. Y. Guslienko, B. A. Ivanov, V. Novosad, Y. Otani, H. Shima, and K. Fukamichi, J. Appl. Phys. **91**, 8037 (2002).

[5] S. B. Choe, Y. Acremann, A. Scholl, A. Bauer, A. Doran, J. Stohr, and H. A. Padmore, Science **304**, 420 (2004).

[6] J. P. Park, P. Eames, D. M. Engebretson, J. Berezovsky, and P. A. Crowell, Phys. Rev. B **67**, 020403(R) (2003).

[7] K. Y. Guslienko, X. F. Han, D. J. Keavney, R. Divan, and S. D. Bader, Phys. Rev. Lett. **96**, 067205 (2006).

[8] S. D. Bader, Rev. Mod. Phys. **78**, 1 (2006).

[9] R. P. Cowburn, Nat. Mater. **6**, 255 (2007).

[10] K. Y. Guslienko, Appl. Phys. Lett. **89**, 022510 (2006).

[11] S. Kasai, Y. Nakatani, K. Kobayashi, H. Kohno, and T. Ono, Phys. Rev. Lett. **97**, 107204 (2006).

[12] B. Van Waeyenberge, A. Puzic, H. Stoll, K. W. Chou, T. Tyliszczak, R. Hertel, M. Fähnle, H. Brückl, K. Rott, G. Reiss, I. Neudecker, D. Weiss, C. H. Back, and G. Schütz, Nature (London) **444**, 461 (2006).

[13] S. Choi, K.-S. Lee, K. Y. Guslienko, and S.-K. Kim, Phys. Rev. Lett. **98**, 087205 (2007).

[14] K.-S. Lee, K. Y. Guslienko, J.-Y. Lee, and S.-K. Kim, Phys. Rev. B (to be published), e-print arXiv:cond-mat/0703538.

[15] R. Hertel, S. Gliga, M. Fähnle, and C. M. Schneider, Phys. Rev. Lett. **98**, 117201 (2007).

[16] K. Yamada, S. Kasai, Y. Nakatani, K. Kobayashi, H. Kohno, A. Thiaville, and T. Ono, Nat. Mater. **6**, 269 (2007).

[17] S.-K. Kim, Y.-S. Choi, K.-S. Lee, K. Y. Guslienko, and D.-E. Jeong, Appl. Phys. Lett. **91**, 082506 (2007).

[18] K. Y. Guslienko, K.-S. Lee, and S.-K. Kim (e-print arXiv: cond-mat: 0708.1359).

[19] A. A. Thiele, Phys. Rev. Lett. **30**, 230 (1973); D. L. Huber, Phys. Rev. B **26**, 3758 (1982).

[20] See http://math.nist.gov/oommf

[21] K. Y. Guslienko (unpublished).

[22] K.-S. Lee, S. Choi, and S.-K. Kim, Appl. Phys. Lett. **87**, 192502 (2005).